



Application of airborne LiDAR to mapping seismogenic faults in forested mountainous terrain, southeastern Alps, Slovenia

Dickson Cunningham,¹ Stephen Grebby,² Kevin Tansey,² Andrej Gosar,^{3,4} and Vanja Kastelic⁵

Received 25 May 2006; revised 10 August 2006; accepted 6 September 2006; published 21 October 2006.

[1] Results are presented of the first airborne LiDAR survey ever flown in Europe for the purpose of mapping the surface expression of earthquake-prone faults. Detailed topographic images derived from LiDAR data of the Idrija and Ravne strike-slip faults in NW Slovenia reveal geomorphological and structural features that shed light on the overall architecture and kinematic history of both fault systems. The 1998 $M_w = 5.6$, and 2004 $M_w = 5.2$ Ravne Fault earthquakes and the historically devastating 1511 $M = 6.8$ Idrija earthquake indicate that both systems pose a serious seismic hazard in the region. Because both fault systems occur within forested terrain, a tree removal algorithm was applied to the data; the resulting images reveal surface scarps and tectonic landforms in unprecedented detail. Importantly, two sites were discovered to be potentially suitable for fault trenching and palaeo-seismological analysis. This study highlights the potential contribution of LiDAR surveying in both low-relief valley terrain and high-relief mountainous terrain to a regional seismic hazard assessment programme. Geoscientists working in other tectonically active regions of the world where earthquake-prone faults are obscured by forest cover would also benefit from LiDAR maps that have been processed to remove the canopy return and reveal the forest floor topography. **Citation:** Cunningham, D., S. Grebby, K. Tansey, A. Gosar, and V. Kastelic (2006), Application of airborne LiDAR to mapping seismogenic faults in forested mountainous terrain, southeastern Alps, Slovenia, *Geophys. Res. Lett.*, 33, L20308, doi:10.1029/2006GL027014.

1. Introduction

[2] High-resolution topographic mapping using airborne LiDAR (Light Detection and Ranging) is an effective method for identifying subtle surface expressions of active faults that pose a potential earthquake hazard. The use of LiDAR to locate faults was pioneered in the Puget lowlands west of Seattle [Haugerud *et al.*, 2003] and along the northern San Andreas fault system [Prentice *et al.*, 2003] where aerial photographs are of limited use in finding and mapping surface fault traces because of thick forest cover. Because the ground return of the LiDAR laser pulse can be

separated from canopy returns, LiDAR data can be processed to virtually deforest the landscape and image the forest floor topography [Haugerud and Harding, 2001]. Here we report the application of LiDAR mapping to image seismogenic strike-slip faults that cut through forested mountainous terrain in the Julian Alps in Slovenia (Figure 1). This is the first reported application of LiDAR to map active fault systems in Europe and to survey high relief alpine landscapes.

[3] The active tectonics of NW Slovenia is driven by the continued northeastward indentation of the NE corner of the Adria microplate [Grenerczy *et al.*, 2005] which is expressed by south-directed thrusting in the Alpine foreland of NE Italy and transpressional and dextral strike-slip deformation in NW Slovenia (Figure 1). Thus, NW Slovenia marks a kinematic transition between E-W striking thrust faults of the Alpine system and NW-striking faults of the Dinaride system, and the exact manner in which dextral strike-slip displacements are transferred to reverse-slip faults in the region is poorly understood [e.g., Carulli *et al.*, 1990]. The NW Slovenian region is characterised by moderate rates of seismicity [Poljak *et al.*, 2000] with three significant earthquakes recorded in the last 30 years (Figure 1): the 1976 Friuli $M_w = 6.4$ event [Perniola *et al.*, 2004], the 1998 $M_w = 5.6$ Bovec-Krn earthquake [Gosar *et al.*, 2001; Zupančič *et al.*, 2001; Bajc *et al.*, 2001] and the 2004 Kobarid $M_w = 5.2$ event [Aoudia *et al.*, 2005]. The largest earthquake ever recorded in the Alps-Dinaride junction was the 1511 western Slovenia earthquake ($M = 6.8$) which was responsible for at least 12,000 deaths. The exact location and mechanism of the 1511 event are debated and no surface ruptures associated with the event have yet been documented [Ribarič, 1979; Fitzko *et al.*, 2005].

[4] The geology of the Julian Alps is dominated by a thick Mesozoic carbonate thrust stack that was transported towards the SSW during the upper-middle Tertiary [Placer, 1998]. Parallel NW-striking Dinaric dextral strike-slip faults such as the Ravne and Idrija faults (Figure 1) cut through the mountains at high angle with apparent disregard for pre-existing topography and older structures formed during Alpine nappe stacking (Figures 2 and 3). The Ravne Fault was responsible for the 1998 and 2004 earthquakes and appears to be an outstanding example of an actively propagating strike-slip fault cutting through pre-existing mountainous terrain [Kastelic and Cunningham, 2006]. Fault plane solutions for both earthquakes show almost pure dextral strike slip displacements on a near-vertical fault with hypocentral depths of 7–9 km [Zupančič *et al.*, 2001]. Although surface ruptures were not observed or expected for either event, the

¹Department of Geology, University of Leicester, Leicester, UK.

²Department of Geography, University of Leicester, Leicester, UK.

³Environmental Agency of the Republic of Slovenia, Ljubljana, Slovenia.

⁴Also at Department of Geology, University of Ljubljana, Ljubljana, Slovenia.

⁵Department of Geology, University of Ljubljana, Ljubljana, Slovenia.

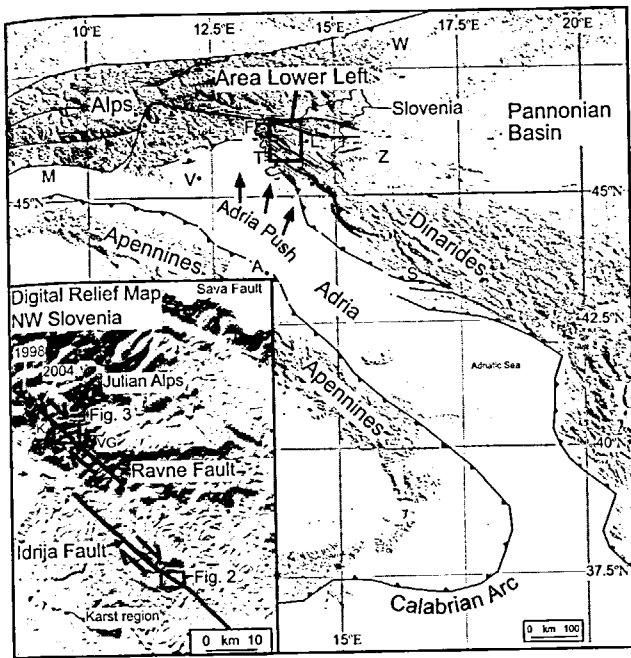


Figure 1. Generalised tectonic map of the Eastern Alps, Dinarides and Adriatic region. Inset map shows locations of Ravne and Idrija Fault segments in NW Slovenia which were mapped by LiDAR and locations of Figures 2 and 3. Location of 1998 Km $M_w = 5.6$, and 2004 Km $M_w = 5.2$ earthquakes also shown. V: Venice; A: Ancona; T: Trieste; L: Ljubljana; Z: Zagreb; S: Split; M: Milan; W: Vienna; F: Friuli; K: Km Mountain; VG: Vogel Mountain. See color version of this figure in the HTML.

total length of the Ravne fault exceeds 35 km and therefore the fault has the potential to produce a much stronger earthquake. Source modelling of the 1998 event indicates that a 13 km long segment of the Ravne Fault was activated NW of the Tolminka Springs Basin in the Km Mountain area (Figure 3) [Bajc *et al.*, 2001]. The Tolminka Springs Basin may therefore act as a weak structural barrier to SE rupture propagation and understanding its internal fault geometry is important for assessing the overall seismic hazard of the Ravne Fault. The Idrija fault occupies a major linear valley traceable on satellite imagery for at least 120 km, but is poorly exposed and no surface scarps have been observed. Both the Ravne and Idrija Faults may have been responsible for the 1511 earthquake [Fitzko *et al.*, 2005]. Instrumental records indicate that the Ravne and Idrija Faults experienced only weak seismicity during the 100 year period prior to 1998.

[5] In this paper, we present first results from airborne LiDAR surveys along the Idrija and Ravne faults which provide the most detailed images yet of the geometry, segmentation, tectonic geomorphology and surface rupturing history of the Idrija and Ravne faults. The LiDAR images are particularly useful for locating possible degraded fault scarps that could be trenched for palaeoseismic analysis and earthquake recurrence interval calculations. In addition, the Ravne survey provides a rare glimpse into the embryonic development of a small

pull-apart basin forming within a high mountainous transpressional orogen.

2. Methodology

[6] Aerial LiDAR surveys were flown in May, 2004 (Idrija survey) and May, 2005 (Ravne survey) by the UK Natural Environment Research Council (NERC) Airborne Remote Sensing Facility Piper Navajo Chieftain aircraft with an Optech ALTM 3033 LiDAR instrument. The Idrija survey covers a swath approximately 2.2 km wide and 23 km long and was flown over a gentle valley containing moderate (<700 m) relief. The Ravne Fault survey covers a swath approximately 2.4 km wide and 17 km long and was flown over rugged mountainous topography along the SE flanks of the Km Range and SW flanks of the Vogel Range with relief along the survey in excess of 1400 m (Figure 1). The LiDAR instrument collects 33,000 laser observations per second and in standard operating mode it collects first pulse, last pulse and intensity data. From an operating altitude above the ground of 600–1000 metres, the resulting height data has an absolute RMS accuracy of better than 15 cm. However, relative accuracy is usually considerably higher. Over particularly rugged terrain, swath width can vary considerably as a function of aircraft

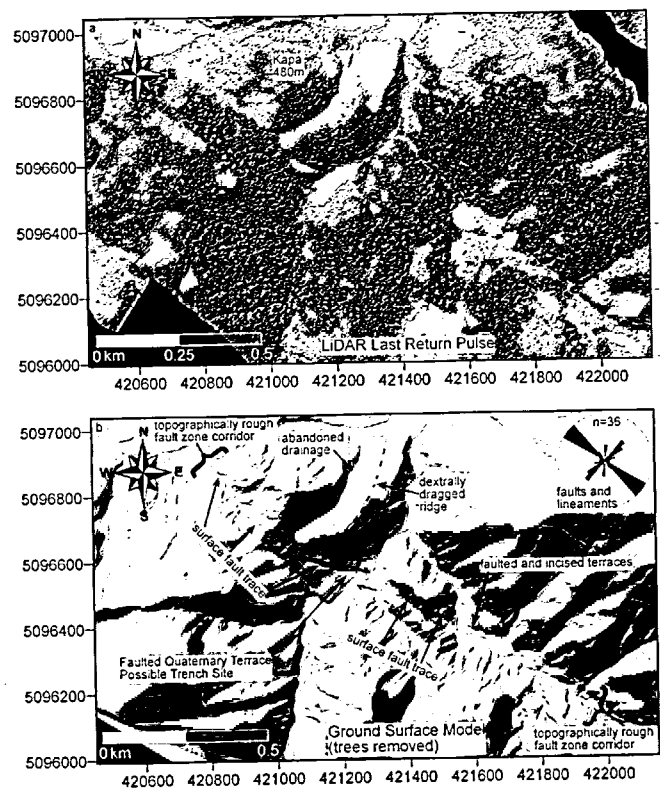


Figure 2. (a) Elevation model created using a nearest neighbour interpolation method from the last pulse signal for the Idrija subset. (b) Result of the tree removal algorithm. Illumination angle = 45° from 330° . Rose diagram shows major fault and lineament trends within scene. Location of image shown in Figure 1. See text for discussion of major features.

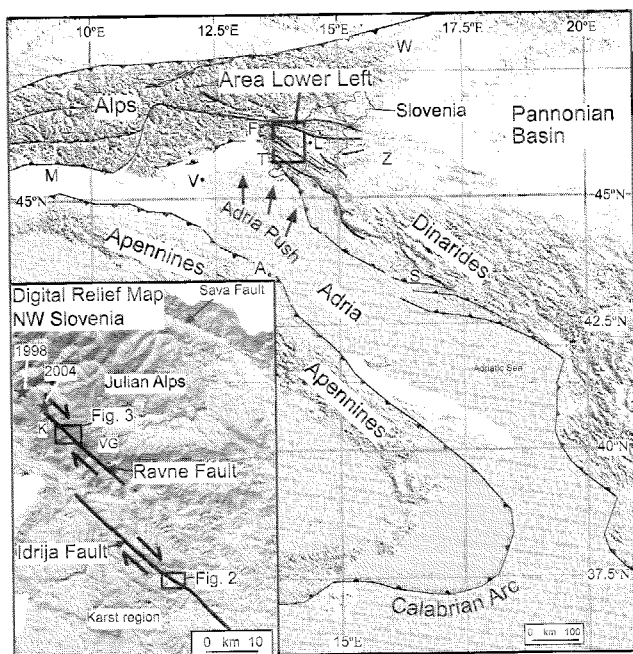


Figure 1. Generalised tectonic map of the Eastern Alps, Dinarides and Adriatic region. Inset map shows locations of Ravne and Idrija Fault segments in NW Slovenia which were mapped by LiDAR and locations of Figures 2 and 3. Location of 1998 Krn $M_w = 5.6$, and 2004 Krn $M_w = 5.2$ earthquakes also shown. V: Venice; A: Ancona; T: Trieste; L: Ljubljana; Z: Zagreb; S: Split; M: Milan; W: Vienna; F: Friuli; K: Krn Mountain; VG: Vogel Mountain. See color version of this figure in the HTML.

total length of the Ravne fault exceeds 35 km and therefore the fault has the potential to produce a much stronger earthquake. Source modelling of the 1998 event indicates that a 13 km long segment of the Ravne Fault was activated NW of the Tolminka Springs Basin in the Krn Mountain area (Figure 3) [Bajc *et al.*, 2001]. The Tolminka Springs Basin may therefore act as a weak structural barrier to SE rupture propagation and understanding its internal fault geometry is important for assessing the overall seismic hazard of the Ravne Fault. The Idrija fault occupies a major linear valley traceable on satellite imagery for at least 120 km, but is poorly exposed and no surface scarps have been observed. Both the Ravne and Idrija Faults may have been responsible for the 1511 earthquake [Fitzko *et al.*, 2005]. Instrumental records indicate that the Ravne and Idrija Faults experienced only weak seismicity during the 100 year period prior to 1998.

[5] In this paper, we present first results from airborne LiDAR surveys along the Idrija and Ravne faults which provide the most detailed images yet of the geometry, segmentation, tectonic geomorphology and surface rupturing history of the Idrija and Ravne faults. The LiDAR images are particularly useful for locating possible degraded fault scarps that could be trenched for palaeoseismic analysis and earthquake recurrence interval calculations. In addition, the Ravne survey provides a rare glimpse into the embryonic development of a small

pull-apart basin forming within a high mountainous transpressional orogen.

2. Methodology

[6] Aerial LiDAR surveys were flown in May, 2004 (Idrija survey) and May, 2005 (Ravne survey) by the UK Natural Environment Research Council (NERC) Airborne Remote Sensing Facility Piper Navajo Chieftain aircraft with an Optech ALTM 3033 LiDAR instrument. The Idrija survey covers a swath approximately 2.2 km wide and 23 km long and was flown over a gentle valley containing moderate (<700 m) relief. The Ravne Fault survey covers a swath approximately 2.4 km wide and 17 km long and was flown over rugged mountainous topography along the SE flanks of the Km Range and SW flanks of the Vogel Range with relief along the survey in excess of 1400 m (Figure 1). The LiDAR instrument collects 33,000 laser observations per second and in standard operating mode it collects first pulse, last pulse and intensity data. From an operating altitude above the ground of 600–1000 metres, the resulting height data has an absolute RMS accuracy of better than 15 cm. However, relative accuracy is usually considerably higher. Over particularly rugged terrain, swath width can vary considerably as a function of aircraft

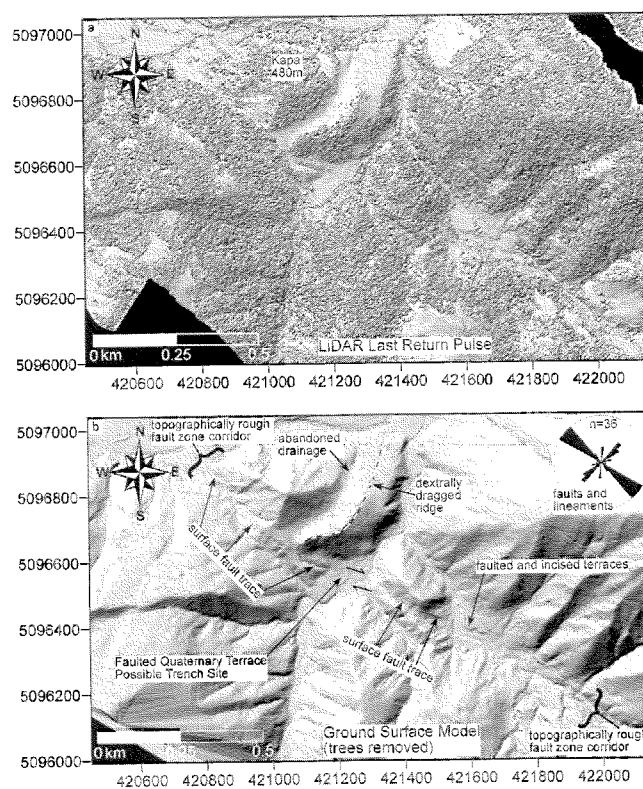


Figure 2. (a) Elevation model created using a nearest neighbour interpolation method from the last pulse signal for the Idrija subset. (b) Result of the tree removal algorithm. Illumination angle = 45° from 330° . Rose diagram shows major fault and lineament trends within scene. Location of image shown in Figure 1. See text for discussion of major features.

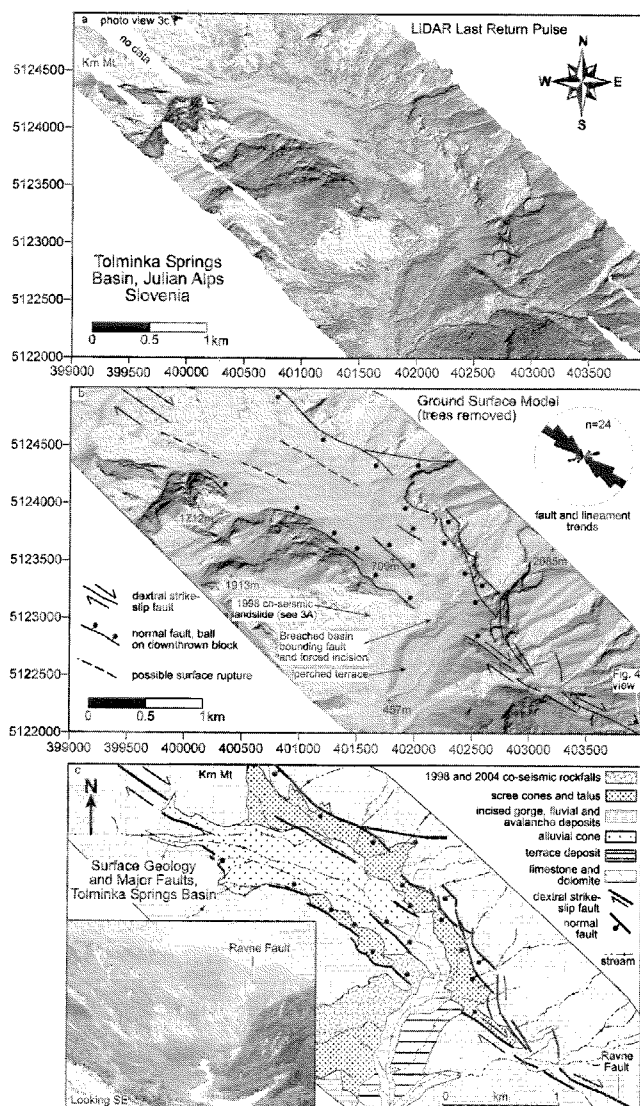


Figure 3. (a) Elevation model created using a nearest neighbour interpolation method from the last pulse signal for the Ravne subset. (b) Result of the tree removal algorithm. Illumination angle = 45° from 150° . Rose diagram shows major fault and lineament trends within scene. (c) A map of surface geology and major faults within the Tolminka Springs Basin based on LiDAR interpretation and follow-on field verification. Location of image shown in Figure 1. Point where photo in Figure 3c was taken shown in Figure 3a. See text for discussion of major features. See color version of this figure in the HTML.

altitude; this may lead to local data gaps between flight lines (on the order of 2–3% in this study).

[7] The LiDAR data for the two surveys consist of xyz (UTM coordinates) and intensity values for both the first and last pulses, in ASCII format. The average point density for the Idrija and Ravne surveys was 1.6 points per square metre. Digital elevation models with grid densities of 2 m were created using a nearest neighbour interpolation method from the last pulse signal. The data were visualised as shaded relief models, and illuminated and viewed from different angles. After visualising the LiDAR data, two sites

were identified for further scrutiny, based on an assessment of the geological and geomorphological features observed in the images. One site in the Idrija survey area, centred on 13.98°E and 46.02°N , contains evidence of surface rupturing and other landscape features typically associated with strike-slip faulting (Figure 2). The location identified for further investigation in the Ravne survey area is centred at 13.73°E and 46.23°N within the Tolminka Springs Basin (Figure 3). In this area, the Ravne Fault cuts through mountainous terrain and splits into several segments that define a small pull-apart basin. Field checks were carried out at both locations to verify features observed in the LiDAR images.

[8] Analysis of the last pulse return data indicated that a significant number of returns were not coming from the ground, but rather from objects in the forest canopy. To resolve this problem, we used an algorithm developed by TerraSolid to compute a surface model based on the generation of Triangulated Irregular Networks (TINs) from known ground return points. Starting at a true ground surface location, the algorithm uses slope angle thresholds to identify other last return pulses that are likely to be ground reflections. Using this method, we were able to successfully remove the majority of non-ground return pulses (tree reflections) and construct a detailed surface model in otherwise forested terrain. A number of limitations of this approach were identified. The main limitation is the incorrect classification of ground and non-ground return pulses [Congalton, 1991; Zhang *et al.*, 2003]. To overcome this limitation, manual confirmation of several cross-sections of LiDAR data was undertaken and outliers removed.

3. Results

[9] The elevation model created using a nearest neighbour interpolation method from the last pulse signal for the Idrija and Ravne subsets are shown in Figures 2a and 3a respectively. Figures 2b and 3b show the surface model that was constructed from known ground returns using TINs for the Idrija and Ravne subsets. The effectiveness of the algorithm to preserve subtle ground features whilst removing false ground returns from canopy objects is clearly seen.

3.1. Idrija Fault Study Area

[10] With trees removed, the Idrija Fault Zone is revealed on the LiDAR image as a topographically rough corridor of deformation with a gullied, irregularly eroded appearance (Figure 2b). Multiple surface fault traces are visible within an approximately 200 m-wide strip that represents the width of the fault damage zone. When plotted on a rose diagram, faults and linear valleys in the Idrija study area follow two dominant trends. The dominant NW trend is typical of Dinaric strike-slip faults in Slovenia. The subordinate NE trend is likely to reflect antithetic sinistral faults that link with the principal displacement corridor. Geomorphic indicators of active faulting include offset fluvial terraces, complex drainage patterns including an abandoned and beheaded stream valley, and possible dextral drag and block rotation adjacent to the fault zone. The segmented nature of the fault zone and its slightly arcuate trace over irregular ground suggests that it dips steeply NE. Steep NE dips for the Idrija Fault are also visible in outcrops SE of Kapa

(Figure 2a) and in underground exposures only 3 km to the SE at the Idrija mercury mine. The area shown in Figure 2 is within a gentle restraining segment of the Idrija Fault where there is a 10° anti-clockwise bend in the regional fault trace from a 308° to 298° trend. Therefore, components of thrusting on dipping fault surfaces should be expected in this area.

[11] Few areas along the Idrija Fault survey show evidence for surface ground rupturing due to a Holocene earthquake. However, in the centre of Figure 2b, a small fluvial terrace has been deposited across the fault zone and subtle shadowing suggests a degraded scarp may be present at the surface. In addition, a slight dextral offset of the main stream channel suggests the fault cuts the terrace. We suggest this may be a good candidate area for fault trenching and palaeoseismic analysis to date previous earthquake events along the SE Idrija Fault and to determine if the fault was the site of the 1511 earthquake.

3.2. Ravne Fault Study Area

[12] With trees removed, the LiDAR image reveals numerous splays of the Ravne Fault System that define the Tolminka Springs Basin (Figures 3 and 4). The fault enters the basin from the SE as a singular strand ('fault trough', Figure 4), but splits and diverges downslope into separate SW and NE basin bounding faults and at least 2 intra-basinal faults. Normal sense of offset is inferred from the overall graben-like topography (photo, Figure 3c) and fault scarps that all face basinwards (Figure 4). Although the Ravne Fault is a dextral fault system overall, strike-slip offsets are not apparent and relief-generating normal sense displacements dominate the image. When plotted on a rose diagram, faults and lineaments in the study area follow the typical Dinaric trend and NE-striking antithetic faults are subordinate (Figure 3b). The Tolminka Springs basin occurs at a gentle 500 m-wide right step along the Ravne Fault system and is a superb example of a localised and active transensional basin constructed within an overall transpressional system. The Krn and Vogel ranges have been stretched apart and the basin floor has been down-dropped and erosionally incised by at least 1200 m.

[13] The oblique 3D perspective of the Tolminka Springs basin (Figure 4) reveals the complex interplay between tectonism, erosion and sedimentation. A large alluvial cone at the NW end of the basin and smaller talus cones along the SW and NE flanks store sediment shed off of the basin margins (Figure 3c). A single river system drains the valley at the SE end and is responsible for removing some accumulated sediment. This river has also eroded a tight canyon outlet through the footwall of the SW border fault. It is clear from the 1200 m+ of relief across the basin, that rates of extension have exceeded basin sedimentation rates (no evidence for glacier carving or morainal sedimentation was identified). However, extension rates are exceeded by fluvial incision rates at the drainage outlet where the main river has cut a steep canyon through older coarse avalanche deposits. The presence of an eroded intra-basinal ridge which is visible in the LiDAR data and was studied in the field (locations labelled 'H' in Figure 4) suggests that the basin outlet was previously dammed by coarse avalanche deposits. Major co-seismic rockfalls in the same area also accompanied the 1998 and 2004 earthquakes (Figure 3).

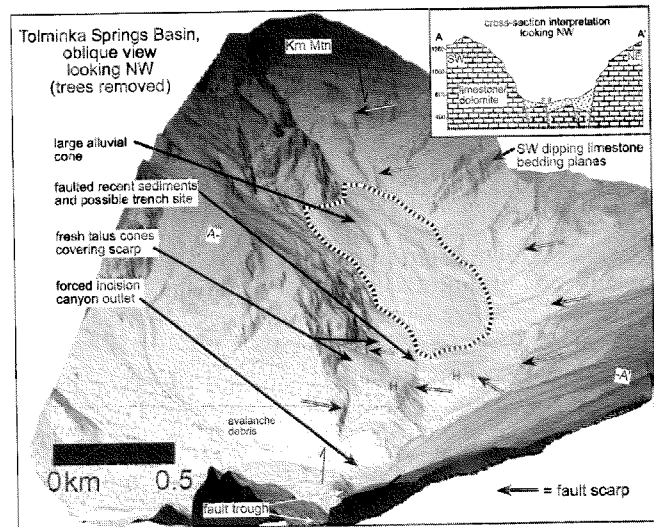


Figure 4. Oblique DEM (last pulse signal, trees removed) of Tolminka Springs Basin along the Ravne Fault, NW Slovenia. View location indicated in Figure 3b (SE corner). Inset shows cross-section (A-A') interpretation of faults responsible for transtensional basin development. 'H' = topographically high remnants of eroded intra-basinal avalanche deposits that may have dammed valley in past.

Dammed drainages would most likely have led to one or more lake bursts in the past contributing to canyon erosion. In addition, the Korita Tolminke gorge 4 km downstream is one of the deepest and steepest defiles in the eastern Alps suggesting flood discharge related downcutting.

4. Implications

[14] On a regional scale, the LiDAR images provide detailed structural information for two of the major faults that accommodate the active strike-slip component of strain along the diffuse NE boundary of the Adria microplate. Both fault systems contain sub-kilometre-wide stepover zones containing multiple fault strands that are responsible for generating youthful topographic landforms that crosscut and modify the older Alpine thrust generated topography. From a future earthquake forecasting perspective, the Idrija stepover at Kapa appears to contain continuously linked faults at the surface without an obvious propagation barrier. However for the Ravne stepover, thick alluvial and talus deposits fill the basin and cover some fault segments making it impossible to prove that faults link across the basin or that the basin acts as a fault propagation barrier. However, a line of scarps revealed on the LiDAR images along the SW margin of the basin is on strike with the Ravne Fault trace where it enters the NW and SE ends of the basin (Figure 3) suggesting that if the Ravne Fault passes continuously through the basin it follows the southwestern basin margin.

[15] The LiDAR images provide the basis for time-efficient follow-on fieldwork to verify fault exposures, check kinematic evidence of movement sense, locate trench sites for palaeoseismological analysis, and distinguish discernible map units and their contacts (Figure 3c). In addition, follow-on fieldwork in the Idrija area revealed

that the topographically rough fault corridor seen on the ground model is the textural expression of brecciation and gouge development; this suggests that other faults may be identifiable using airborne LiDAR simply by their textural expression. In addition, oblique perspective views of the LiDAR data clearly revealed the attitude of folded bedding in steep terrain (Figure 4) which was later verified in the field.

[16] The LiDAR images for the Idrija and Ravne fault systems are the most detailed views of the topographic expression of active faults in NW Slovenia ever produced. Because the last pulse data are insufficient to resolve the surface elevation model, it was essential to apply a tree removal algorithm; the improvement in visualising the ground surface is demonstrated by the striking contrast between the Idrija last pulse image and the tree-removed image (Figure 2). LiDAR surveys can be flown over flat or mountainous terrain, although mountainous terrain provides challenges for pilots and may force a higher altitude survey and lower pixel resolution. Nevertheless, the usefulness of incorporating LiDAR surveys into a seismic risk analysis is demonstrated in cases from the western US and now Europe. Geoscientists working in other tectonically active regions of the world where earthquake-prone faults are obscured by forest cover such as the Apennines, Pyrenees, New Zealand, Nepal, Assam, Indonesia, Ecuador, Peru, etc, would also benefit from LiDAR maps that have been processed to remove the canopy return and reveal the forest floor topography.

[17] **Acknowledgments.** This work was supported by NERC ARSF grant MC04/09 and Royal Society grant 28/D/23901/SM awarded to D. Cunningham. Initial data processing was carried out by staff at the University of Cambridge, Unit for Landscape Modelling. Andrej Gosar is grateful to the Surveying and Mapping Authority of Slovenia and to the Geodetic Institute of Slovenia for GPS base station assistance during the LiDAR surveys. The authors would like to thank Andrew Anstee and Ned Chisholm at Infoterra Ltd., UK for software support and advice.

References

- Aoudia, A., A. Zille, A. Borghi, R. Riva, R. Barzaghi, M. Živčić, and G. Panza (2005), The July 2004 Western Slovenia earthquake: From localised fault-scale complexities to distributed deformation at the junction between the south-eastern Alps and External Dinarides, *Geophys. Res. Abstr.*, **7**, 09258.
- Bajc, J., A. Aoudia, A. Sarao, and P. Suhadolc (2001), The 1998 Bovec-Krn mountain (Slovenia) earthquake sequence, *Geophys. Res. Lett.*, **28**, 1839–1842.
- Carulli, G. B., R. Nicolich, A. Rebez, and D. Slejko (1990), Seismotectonics of the Northwest External Dinarides, *Tectonophysics*, **179**, 11–25.
- Congalton, R. G. (1991), A review of assessing the accuracy of classifications of remotely sensed data, *Remote Sens. Environ.*, **37**, 35–46.
- Fitzko, F., P. Suhadolc, A. Aoudia, and G. F. Panza (2005), Constraints on the location and mechanism of the 1511 Western Slovenia earthquake from active tectonics and modeling of macroseismic data, *Tectonophysics*, **404**, 77–90.
- Gosar, A., R. Stopar, M. Car, and M. Mucciarelli (2001), The earthquake on 12 April, 1998 in Krn mountains (Slovenia): Ground motion amplification study using microtremors and modelling based on geophysical data, *J. Appl. Geophys.*, **47**(2), 153–167.
- Grenerczy, G., G. Sella, S. Stein, and A. Kenyeres (2005), Tectonic implications of the GPS velocity field in the northern Adriatic region, *Geophys. Res. Lett.*, **32**, L16311, doi:10.1029/2005GL022947.
- Haugerud, R. A., and D. J. Harding (2001), Some algorithms for virtual deforestation (VDF) of lidar topographic survey data, *Int. Arch. Photogramm. Remote Sens.*, **XXXIV-3/W4**, 211–217.
- Haugerud, R., D. J. Harding, S. Y. Johnson, J. L. Harless, C. S. Weaver, and B. L. Sherrod (2003), High-resolution lidar topography of the Puget Lowland, Washington—A bonanza for Earth science, *GSA Today*, **13**, 4–10.
- Kastelic, V., and D. Cunningham (2006), Multi-disciplinary investigation of active strike-slip fault propagation in the Julian Alps: The Ravne Fault, NW Slovenia, *Geophys. Res. Abstr.*, **8**, 05018.
- Perniola, B., G. Bressan, and S. Pondrelli (2004), Changes in failure stress and stress transfer during the 1976–77 Friuli earthquake sequence, *Geophys. J. Int.*, **156**, 297–306.
- Placer, L. (1998), Contribution to the macrotectonic subdivision of the border region between southern Alps and External Dinarides, *Geologija*, **41**, 223–255.
- Poljak, M., M. Živčić, and P. Zupančič (2000), The seismotectonic characteristics of Slovenia, *Pure Appl. Geophys.*, **157**, 27–55.
- Prentice, C. S., C. J. Crosby, D. J. Harding, R. A. Haugerud, D. J. Merritts, T. Gardner, R. D. Koehler, and J. N. Baldwin (2003), Northern California LiDAR data: A tool for mapping the San Andreas fault and Pleistocene marine terraces in heavily vegetated terrain, *Eos Trans. AGU*, **84**(46), Fall Meet. Suppl., Abstract G12A-06.
- Ribarič, V. (1979), The Idrija earthquake of March 26, 1511—A reconstruction of some seismological parameters, *Tectonophysics*, **53**, 315–324.
- Zhang, K., S.-C. Chen, D. Whitman, M.-L. Shyu, J. Yan, and C. Zhang (2003), A progressive morphological filter for removing nonground measurements from airborne LIDAR data, *IEEE Trans. Geosci. Remote Sens.*, **41**, 872–882.
- Zupančič, P., I. Ceci, A. Gosar, L. Placer, M. Poljak, and M. Živčić (2001), The earthquake of 12 April 1998 in the Krn Mountains (Upper Soča valley, Slovenia) and its seismotectonic characteristics, *Geologija*, **44**(1), 169–192.
- D. Cunningham, Department of Geology, University of Leicester, Leicester LE1 7RH, UK. (wdc2@le.ac.uk)
- A. Gosar, Environmental Agency of the Republic of Slovenia, SI-1000 Ljubljana, Slovenia.
- S. Grebbly and K. Tansey, Department of Geography, University of Leicester, Leicester LE1 7RH, UK.
- V. Kastelic, Department of Geology, University of Ljubljana, SI-1000 Ljubljana, Slovenia.